

## Formation of magnetic nanocolumns during vapor phase deposition of a metal-polymer nanocomposite: Experiments and kinetic Monte Carlo simulations

L. Rosenthal, H. Greve, V. Zaporozhchenko, T. Strunskus, F. Faupel et al.

Citation: *J. Appl. Phys.* 114, 044305 (2013); doi: 10.1063/1.4816252

View online: <http://dx.doi.org/10.1063/1.4816252>

View Table of Contents: <http://jap.aip.org/resource/1/JAPIAU/v114/i4>

Published by the AIP Publishing LLC.

---

### Additional information on J. Appl. Phys.

Journal Homepage: <http://jap.aip.org/>

Journal Information: [http://jap.aip.org/about/about\\_the\\_journal](http://jap.aip.org/about/about_the_journal)

Top downloads: [http://jap.aip.org/features/most\\_downloaded](http://jap.aip.org/features/most_downloaded)

Information for Authors: <http://jap.aip.org/authors>

## ADVERTISEMENT



**AIPAdvances**

Now Indexed in Thomson Reuters Databases

Explore AIP's open access journal:

- Rapid publication
- Article-level metrics
- Post-publication rating and commenting

# Formation of magnetic nanocolumns during vapor phase deposition of a metal-polymer nanocomposite: Experiments and kinetic Monte Carlo simulations

L. Rosenthal,<sup>1,a)</sup> H. Greve,<sup>2,b)</sup> V. Zaporozhchenko,<sup>2,c)</sup> T. Strunskus,<sup>2</sup> F. Faupel,<sup>2,d)</sup> and M. Bonitz<sup>1</sup>

<sup>1</sup>*Institut für Theoretische Physik und Astrophysik, Christian-Albrechts-Universität zu Kiel, Leibnizstraße 15, D-24098 Kiel, Germany*

<sup>2</sup>*Institut für Materialwissenschaft, Lehrstuhl für Materialverbunde, Christian-Albrechts-Universität zu Kiel, Kaiserstraße 2, D-24143 Kiel, Germany*

(Received 18 April 2013; accepted 4 July 2013; published online 24 July 2013)

Metal-polymer nanocomposites have been investigated extensively during the last years due to their interesting functional applications. They are often produced by vapor phase deposition which generally leads to the self-organized formation of spherical metallic nanoparticles in an organic matrix, while nanocolumns are only obtained under very specific conditions. Experiments [Greve *et al.* Appl. Phys. Lett. **88**, 123103 (2006)] have shown that co-evaporation of the metallic and organic components in a simple single-step process can give rise to the formation of ultrahigh-density Fe-Ni-Co nanocolumnar structures embedded in a fluoropolymer matrix. Here we present a kinetic Monte Carlo approach which is based on a new model involving the depression of the melting point on the nanoscale and a critical nanoparticle size required for solidification. In addition we present new experimental results on the formation of Fe-Ni-Co nanocolumns in a Teflon AF matrix via co-evaporation down to a deposition temperature of  $-70^{\circ}\text{C}$  and also report the magnetic properties of the nanocolumns. The simulations provide a detailed understanding of the transition from spherical cluster growth to formation of elongated structures and are in good agreement with the experiments. © 2013 AIP Publishing LLC. [<http://dx.doi.org/10.1063/1.4816252>]

## I. INTRODUCTION

Nanocomposites containing metallic nanoparticles in a dielectric polymer matrix have very interesting functional applications ranging from plasmonics<sup>2,3</sup> and high-frequency magnetic materials<sup>4</sup> to antibacterial coating<sup>5,6</sup> (for recent reviews see Ref. 7–9). Such metal-polymer nanocomposites are often produced by vapor-phase co-deposition of the metallic and organic components,<sup>10–12</sup> since this allows for tailoring of the nanoparticle filling factor and other parameters. Even alloy nanoparticles with well-defined composition can be incorporated.<sup>13</sup> During co-deposition, metallic nanoparticles form via self-organization since the metal has a much higher cohesive energy than the organic component and the interaction energy between the two components is very low (except for very reactive metals). One can assume that the self-organization mechanism during the deposition of polymer-based nanocomposites is analogous to metal cluster formation on a polymer surface.<sup>14</sup> When energetic metal atoms impinge on the polymer surface, they undergo various processes including a random walk on the surface, diffusion into the bulk, and desorption.<sup>15,16</sup> Within their diffusion distance, metal atoms may encounter each other or may be captured by a surface defect. This leads to aggregation and formation of metal clusters which are embedded into the

polymer matrix upon growth of the nanocomposite film. The metal filling factor depends on the condensation coefficient of metal atoms on a given polymer surface<sup>17</sup> as well as on the metal-polymer deposition ratio.<sup>18</sup> In these terms, the volume fractions of metallic nanoparticles in the composite films can be easily controlled through the ratio  $\kappa = R_m/R_p$  of the deposition rates of metal and polymer components,  $R_m$  and  $R_p$ , respectively.

Generally, the nanoparticles obtained upon vapor phase co-deposition have a spherical shape (as long as the filling factor is low enough to prevent nanoparticle coalescence). This is expected from the minimization of the surface energy and the above mentioned formation process. However, under specific conditions, involving a very high deposition rate ratio  $\kappa$  and a very low metal condensation coefficient, formation of elongated Fe-Ni-Co (Ref. 1) and Au (Ref. 19) nanocolumns has been reported in a Teflon AF (amorphous fluoropolymer, Dupont<sup>TM</sup>) matrix. While the formation process of the spherical nanoparticles is well understood and has also been modeled by kinetic Monte Carlo (KMC) simulations,<sup>20–24</sup> only a crude qualitative model was suggested for nanocolumn formation.<sup>1</sup> According to this model, a very low condensation coefficient is crucial. Thus the metal atoms arriving on the growing nanocomposite film from the gas phase will stick whenever they encounter a growing metallic nanoparticle but will have a very large surface diffusivity and a high thermal desorption probability if they impinge on the organic matrix, due to the very low metal-organic interaction energy. On the organic surface, there is a

<sup>a)</sup>Electronic mail: rosenthal@theo-physik.uni-kiel.de

<sup>b)</sup>Present address: NXP Semiconductors, Hamburg, Germany.

<sup>c)</sup>Deceased.

<sup>d)</sup>Electronic mail: ff@tf.uni-kiel.de

competition between thermal desorption, diffusion, and trapping at a nanoparticle. In these terms, it was proposed that beyond a critical deposition rate ratio  $\kappa_{cr}$ , direct impingement of newly arriving metal atoms from the gas phase gives rise to a growth of metal nanoparticles in the direction perpendicular to the surface that is faster than their embedding into the growing organic matrix. However, kinetic Monte Carlo simulations using this concept failed to reproduce the experimental results even in a qualitative manner.

Here we report new experimental results on the formation of Fe-Ni-Co nanocolumns in a Teflon AF matrix via co-evaporation, which extend the temperature range of the previous experiments down to  $-70^\circ\text{C}$  and include the characterization of the highly anisotropic magnetic properties. In addition, we propose a new model for nanocolumn formation and we present new substantially improved kinetic Monte Carlo simulations which are able to explain the experimental results not only qualitatively but even quantitatively. A key new aspect of the present model is solidification of the nanoparticles at a critical size, which drastically slows down the kinetics for the establishment of the spherical equilibrium shape.

## II. EXPERIMENTS

The nanocomposite films of a thickness from 100 nm to 200 nm were produced by co-evaporation of the organic and metallic components on Si wafers using a homemade high vacuum deposition chamber.<sup>1,25</sup> Teflon AF (granulates, Dupont) and Fe-Ni-Co wires of diameter 1 mm and 99.99% purity (Good Fellow Industries, U.K.) were used as starting materials. For preparation of samples for transmission electron microscopy (TEM) and magnetic characterization, polymer foils (Upilex-S<sup>®</sup>) were used as substrates. Polymers generally do not lend themselves for evaporation because they decompose upon heating, however, for some polymers, such as Teflon AF, the monomer structure is preserved upon thermal breaking of the covalent bonds along the backbone chain of the polymer, and a Teflon AF film can be deposited which differs from the starting material mainly by its much lower molecular weight. The molecular weight reduction is not critical for functional applications. A detailed discussion of the properties of Teflon AF can be found in Refs. 25 and 26.

Deposition rates of 0.15–0.3 nm/min and 0.6–1 nm/min were typically used for Teflon AF and Fe-Ni-Co, respectively. The metallic volume filling factor  $f$  of the nanocomposites was determined by energy dispersive X-ray spectroscopy (EDX) as described in Ref. 12. The experimental error of  $f$  is  $\pm 20\%$ . The magnetic measurements were carried out with a LakeShore 7300 vibrating sample magnetometer (VSM). For further experimental details see Refs. 1, 25, and 26. Fig. 1 shows the metal volume filling factor  $f$  as a function of the deposition rate ratio  $\kappa$  for deposition at different substrate temperatures. At the highest temperatures, one notes a sharp increase of the filling factor above a certain value of  $\kappa$ . For lower substrate temperatures, the increase of  $f$  shifts to lower  $\kappa$  and is more smeared out, which is most pronounced at  $-70^\circ\text{C}$ . At this temperature the data were fitted to the function

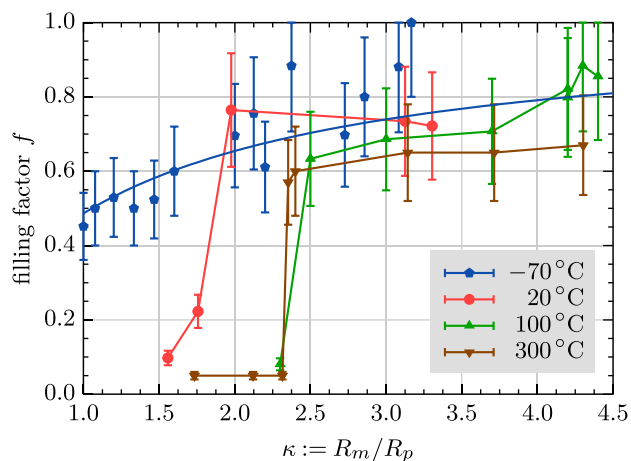


FIG. 1. Experimental results of the volume filling factor  $f$  as a function of the deposition rate ratio  $\kappa$  of Fe-Ni-Co and Teflon AF, for different temperatures.

$$f = \frac{\kappa C}{\kappa C + 1}, \quad (1)$$

where the fitting parameter  $C$  is the metal condensation coefficient. Eq. (1) follows immediately by expressing  $f$  in terms of the effective deposition rates which are multiplied by the condensation coefficients, taking into account metal desorption, and assuming complete condensation for the organic component. The fit yields  $C = 0.94 \pm 0.08$ , in good agreement with the expectation that the condensation coefficient approaches unity at low temperatures.<sup>27</sup> It has to be pointed out, however, that the condensation coefficient depends on the metal coverage at the surface of the growing composite and, hence, on  $\kappa$  because metal atoms stick with a probability of unity if they directly impinge on a metal nanoparticle or if they reach a metal nanoparticle via surface diffusion. Therefore, Eq. (1) is not applicable at higher temperatures, where the condensation coefficient on Teflon AF is expected to be very low.<sup>17,27</sup> Even the value of  $C = 0.94$  obtained at  $-70^\circ\text{C}$  probably overestimates the condensation coefficient for the pure polymer.

The microstructure was investigated by means of transmission electron microscopy. Representative TEM micrographs are displayed in Figs. 2 and 3 (see Ref. 26 for further details). Fig. 2 shows cross-sectional images of a nanocomposite prepared at  $160^\circ\text{C}$ . (As described in Ref. 26, the nanocomposite film was grown on top of an evaporated Teflon

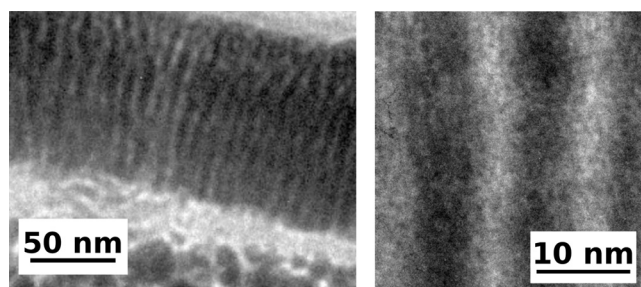


FIG. 2. Left: Cross-sectional TEM image showing the formation of Fe-Ni-Co nanocolumns in Teflon AF on top of a layer of Ag clusters in Teflon AF, isolated by 20 nm of the same matrix material. Right: Cross-sectional higher magnified TEM image of self-organized nanocolumns of Fe-Ni-Co in Teflon AF.

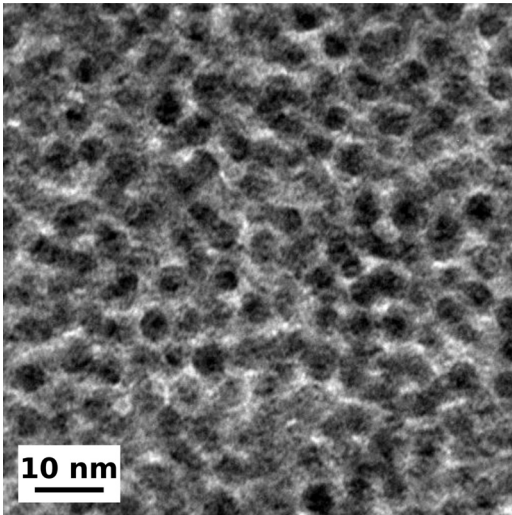


FIG. 3. Top-view TEM micrograph showing Fe-Ni-Co nanocolumns in a Teflon AF matrix. The nanocomposite was deposited at a low substrate temperature of  $-70^{\circ}\text{C}$  on an electron transparent TEM grid which was covered with a Teflon AF layer prior to the nanocomposite deposition, in order to exclude substrate effects.<sup>26</sup>

AF film containing spherical silver nanoparticles. In order to exclude any influence of the silver particles on the growth of the magnetic nanocolumns, a Teflon AF separation layer of 20 nm was evaporated on top of the Ag-Teflon AF nanocomposite film before the layer of Fe-Ni-Co-Teflon AF nanocomposite was deposited.) It is obvious from Fig. 2 that the Fe-Ni-Co nanoparticles have grown as nanocolumns with a diameter of about 7–8 nm and a length extending through the whole film, resulting in an aspect ratio well above 10. The deposition was performed under conditions of normal incidence, and the orientation of the nanocolumns is perpendicular to the substrate. Experiments were also carried out with normal incidence of the organic component and with an incident angle of  $55^{\circ}$  with respect to the substrate for the metallic component. Under these conditions, the resulting nanocolumns were inclined with an angle of  $70^{\circ}$ – $75^{\circ}$  with respect to the substrate, indicating that the growth direction can be controlled via the angle of incidence. Fig. 3 shows a top-view TEM micrograph of a nanocomposite film deposited at

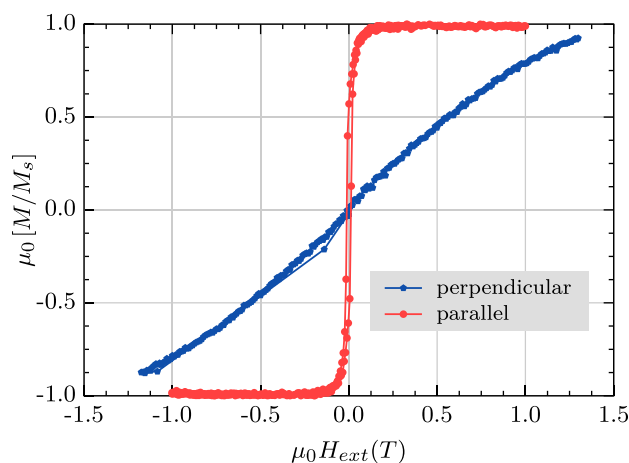


FIG. 4. Hysteresis curves for a Fe-Ni-Co-Teflon AF nanocomposite film co-evaporated at  $300^{\circ}\text{C}$  substrate temperature. One notes a strong magnetic anisotropy with the easy axis of magnetization parallel to the film plane.

$-70^{\circ}\text{C}$ . The film has a thickness of 30 nm to ensure electron transparency. Evidence for the nanocolumnar shape of the metallic particles is provided from the fact that no overlap of particles is seen. For spherical particles of about 5 nm diameter, the electron beam would have a high probability to penetrate through more than one particle, giving the impression of coalesced particles as always seen in top-view images under the present conditions for spherical particles.<sup>7,28</sup>

The highly anisotropic nanocolumnar structure is also reflected in highly anisotropic magnetic properties. Hysteresis curves for a sample deposited at  $300^{\circ}\text{C}$  are shown in Fig. 4. One notes a completely different behavior for measurements parallel and perpendicular to the film plane. The very soft magnetic behavior parallel to the film is a clear signature of magnetization reversal by domain wall movement, whereas saturation in the perpendicular direction requires very high fields indicating that magnetization reversal is only possible without domain wall movement.<sup>29</sup> Apparently, the magnetization of the nanocolumns is different from the case of a long isolated column, cf. Fig. 5(a), where shape anisotropy always leads to an orientation of the easy axis parallel to the column, and reveals the presence of domain walls perpendicular to the long column axis, cf. Fig. 5(b).

The observed magnetization behavior can be explained in terms of a competition of de-magnetizing fields and dipole-dipole fields. It has been shown, e.g., for arrays of much larger Co nanowires electro-deposited in anodic alumina, that the magnetization can be tuned parallel or perpendicular to the nanowires by changing their length.<sup>30</sup> In the present case, the dipole-dipole interaction dominates the behavior due to the small nanocolumn separation of only a few nanometers.

### III. KINETIC MONTE CARLO SIMULATIONS

The KMC simulations described below are based on previous simulations of diffusion and growth of metal clusters in a polymer matrix.<sup>20–24</sup> As it is usual for KMC simulations, the investigated system is modeled in terms of a few idealized elementary processes which are crucial for the long-time dynamics. The time evolution can then be generated with this set of elementary processes and their

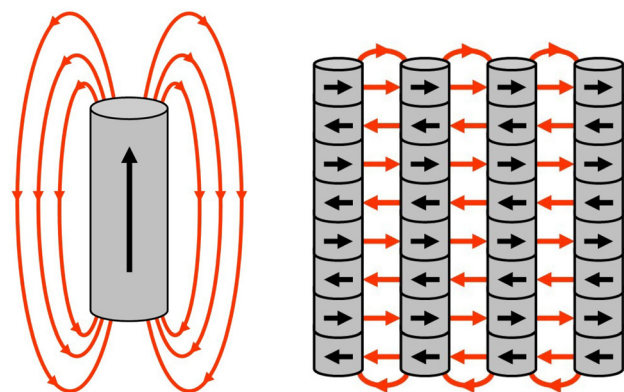


FIG. 5. Left: Sketch of the magnetization in an isolated long magnetic nanocolumn, where the easy axis of magnetization is parallel to the column due to shape anisotropy. Right: In an array of nanocolumns with strong dipole-dipole coupling, the easy axis is oriented perpendicular to the nanocolumns, and magnetic domain walls are incorporated.

corresponding rates, treating them as random processes. In case of metal-polymer nanocomposite formation the main processes are surface diffusion, evaporation of monomers and the formation of clusters and nanocolumns, respectively. To derive a practical simulation algorithm we used the following assumptions: The atomic and chemical structure of the polymer matrix is essentially neglected. Instead, the influence of the substrate is reflected in averaged cluster mobilities (expressed in terms of rate constants) and diffusion jump lengths of clusters. The polymer is assumed to be a continuum with periodic boundary conditions in the  $x$ - and  $y$ -direction (parallel to the surface).

Metal atoms and clusters are modeled within the framework of the liquid drop model. They are considered as spheres with constant density regardless of their size, where a single atom is assumed to have a radius  $r_1 = 0.145$  nm. Furthermore, clusters are assumed to be stable in the sense that they do not decompose into smaller clusters. Atoms are deposited randomly on the surface and immediately start to perform isotropically distributed surface diffusion jumps with a diffusion frequency  $\nu_s$  and an averaged diffusion jump length  $l$  which is chosen to be  $l = 0.6$  nm, which is approximately the diameter of a polymer chain. Clusters (including monomers) obey two different growth mechanisms: the first one, for liquid clusters, is the fusion of two clusters to a larger one according to the reaction scheme  $M_n + M_m \rightarrow M_{n+m}$ , where the subscript labels the number of atoms the cluster consists of. Merging of clusters occurs when the distance of two clusters falls below half of the jump length (0.3 nm) and is assumed to take place without any finite equilibration time. Thus, in the simulations the spherical shape of the new cluster is reached immediately after contact of the two constituting clusters. The second growth mechanism is the one that gives rise to the formation of elongated nanocolumns growing in the direction perpendicular to the surface. In our simulation, it is initiated whenever the radius of one of two merging clusters is above the melting radius  $r_m$ , i.e., when the number of atoms  $N$  exceeds a certain value  $N_m$ . This growth occurs, for instance, when a monomer impinges directly into the interaction region of a pre-existing cluster with  $N > N_m$  atoms which is partially buried by the surface. This process also occurs when a cluster merges with a partially buried cluster as a result of surface diffusion. We assume that the new cluster does not reach a spherical shape after equilibration. Instead, the incoming cluster coalesces with the part of the buried cluster which extends above the surface.

These growth mechanisms are subject to two boundary conditions: The first one is volume conservation (due to the assumption of constant density). Furthermore the points  $P_1$  and  $P_2$  in Fig. 6 (denoting the circular intersection line of the cluster with the surface) are assumed to remain immobile. Hence the resulting initial column consists of two spherical caps separated by the surface dividing the column into a buried part and a part located above the surface. We note that the intersection line of the clusters with the surface moves upwards during the deposition process due to the arrival of new organic molecules. These two mechanisms of nanocolumn growth are depicted in Fig. 6. These mechanisms can

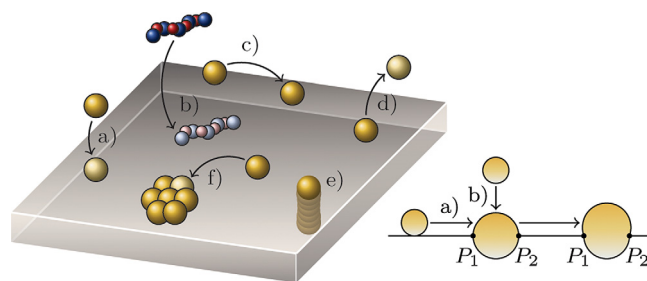


FIG. 6. Left: Sketch of the cluster processes included in the KMC-simulations: deposition of monomers (a) and polymer (b), surface diffusion of clusters (c), evaporation of monomers (d), formation of metallic nanocolumns (e), cluster growth induced by surface diffusion (f). Right: Illustration of the two basic mechanisms of nanocolumn growth: (a) growth induced by surface diffusion and (b) by direct impingement of a monomer on a preexisting cluster. The polymer surface moves upwards during the deposition process due to arrival of new organic molecules from the gas phase.

repeat the same way with a free cluster and a pre-existing column where only the upper part of the column is involved into the growth process.

To incorporate the effect of very low condensation coefficients  $C$  known for metals on Teflon AF,<sup>17,27</sup> monomers are allowed to evaporate from the surface with a certain rate constant  $\nu_e$ . The constant  $\nu_e$  is given in units of the surface diffusion rate  $\nu_s$  and is adjusted to the experimental values of  $C$ . To model metal deposition, in the simulations metal atoms are randomly placed on the surface of the matrix with a constant deposition rate  $R_m$ . A metal thickness of the diameter of a single atom corresponds to the amount of one monolayer (ML) of atoms which is defined to have a number density of 10 atoms per  $\text{nm}^2$ . Simultaneously with the deposition of metal atoms a constant shift of the surface in  $z$ -direction with a certain rate  $R_p$  is applied to model the co-deposition process.<sup>24</sup> Both rates are given in units of  $\text{nm/s}$ .

Unfortunately, very little is known about the rates of surface diffusion of clusters on and evaporation of monomers from Teflon AF. For that reason, we decided not to incorporate the temperature in our simulations (e.g., via an Arrhenius law, as it is usual in KMC simulations). Instead, we treated the main input parameters (e.g., surface diffusion and evaporation rate of monomers and the melting radius  $r_m$ ) as free parameters to achieve the best overall agreement with the experiments. To incorporate the size-dependence of the surface diffusion coefficients  $D_n$  of metal clusters, we used a power law dependence on the cluster size  $n$ ,  $D_n = n^{-1}D_1$ , which is known from MD simulations of cluster diffusion on crystalline surfaces.<sup>31</sup>

#### IV. SIMULATION RESULTS

To check the applicability of our simulation model we performed simulations over a broad range of parameters. For all results presented below, the composites have a finite thickness of 100 nm and a surface cross section of  $350 \text{ nm} \times 350 \text{ nm}$ . The metal deposition rate  $R_m$  was kept at a constant value of 1.5 nm/min, and the deposition rate ratio  $\kappa$  was varied by tuning the polymer deposition rate  $R_p$  to the desired value. The melting radius  $r_m$  of the clusters was treated as a free parameter. For the surface diffusion coefficient of monomers  $D_1$  and the evaporation rate  $\nu_e$

of monomers, we used the following parameter range that is motivated by experiments:  $D_1 = 1 \times 10^{-11} \dots 2 \times 10^{-10} \text{ cm}^2/\text{s}$  and  $\nu_e = 1 \times 10^3 \dots 2 \times 10^4 \text{ s}^{-1}$ . In order to obtain good statistics, the results presented below are averaged over 20 runs with a constant parameter set but different initial conditions. The deviations were usually less than one percent, so no error bars are included in the figures. The focus of our investigations lies on the influence of the atomic evaporation rate (desorption from the surface) and the surface diffusion rate, which depend on the metal-polymer interaction and hence on the condensation (or sticking) coefficient  $C$ . A low value of  $C$  is accompanied by a large diffusion length.

The main effect which was observed during experiments is a dramatic increase of the volume filling factor  $f$  with the deposition rate ratio  $\kappa$ . In contrast to the experiments, the simulations provide additional data, such as the size distribution of clusters, their spatial distribution as well as the exact number of the nanocolumns. This allows for a more complete understanding of the self-organized process of nanocolumn growth.

In Fig. 7 simulation results of different quantities are shown as a function of the deposition rate ratio  $\kappa$ , for a system with a surface area of  $350 \text{ nm} \times 350 \text{ nm}$  and a final thickness (after the termination of both deposition processes) of  $100 \text{ nm}$ . The simulations clearly show a strong increase of the metal filling factor  $f$  for values of  $\kappa \geq 1.5$  which is related to the formation of nanocolumns cf. Figs. 7(a) and 7(c). The upper panel of Fig. 7 which shows the number of nanocolumns indicates that there is a sharp transition from the pure spherical growth regime to a regime of column growth that coincides with the strong increase of the filling factor. Within our model the explanation of this phenomenon

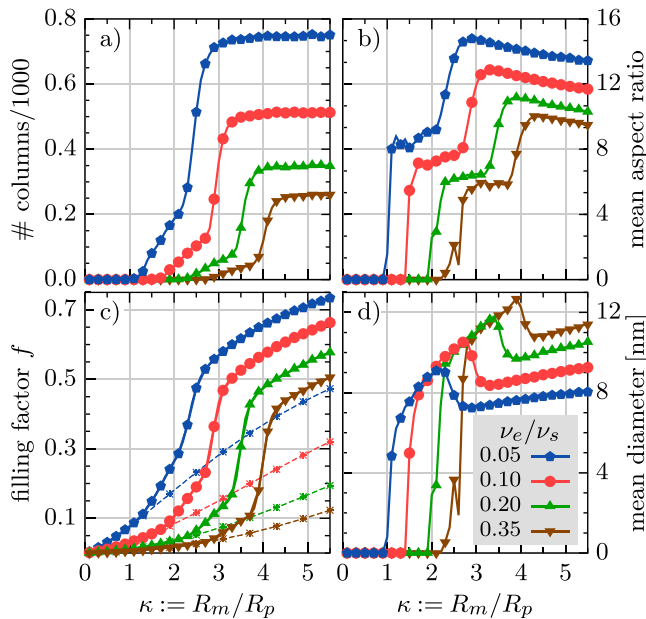


FIG. 7. Nanocolumn properties as a function of the deposition rate ratio  $\kappa$ , for four different values of the evaporation rate  $\nu_e$ . The melting radius  $r_m$  was set to  $2.23 \text{ nm}$  and the monomer surface diffusion coefficient  $D_1$  to  $1.845 \times 10^{-11} \text{ cm}^2/\text{s}$  (corresponding to the rate  $\nu_s = 2.05 \times 10^4 \text{ s}^{-1}$ ). The figure parts show (a) the total number of nanocolumns, (b) the mean aspect ratio (defined as the ratio of the mean length to the mean diameter of the columns), (c) the metal filling factor with (solid lines) and without (dashed lines) column growth (d) the mean column diameter.

is as follows: When atoms impinge on the surface, they may undergo various competing processes like surface diffusion, re-emission and nucleation after encountering each other. One crucial point for the observed transition is the low condensation coefficient of metal on Teflon AF, which is caused by the weak chemical interaction of the two components. Metal atoms (clusters) have to encounter each other and form nuclei that can be stabilized in the polymer matrix and initiate the column growth. The simultaneous deposition of the polymer matrix works against the growth of nuclei and isolates the clusters from each other. For low values of  $\kappa$  the re-emission of atoms and the growth of the polymer matrix are the dominant processes and prevent the growth of clusters that are big enough to initiate column growth. When  $\kappa$  exceeds a critical value, the deposition of metal atoms plays the dominant role and the re-emission and isolation of clusters by the growing matrix is compensated by agglomeration of atoms with pre-existing clusters. As a consequence, the growth of clusters is strongly accelerated and some clusters reach the critical cluster size to initiate column growth.

### A. Effect of atomic desorption

In Fig. 7 we analyze how the filling factor and geometrical properties of the nanocolumns are affected by the evaporation rate  $\nu_e$  and the deposition rate ratio. The whole range of investigated values of  $\kappa$  can be divided into four regions: The first region is characterized by pure spherical growth and an almost linear increase of the metal filling factor, see Fig. 7(c). In the second region column growth sets in, see Fig. 7(a). With an increasing desorption rate and the concomitant increase in the surface diffusivity, the filling factor starts to increase nonlinearly and the transition to the columnar growth regime is shifted to larger values of  $\kappa$ , cf. Fig. 7(a). This effect can be easily understood in terms of the underlying column growth model: As explained in Sec. III, clusters have to grow beyond the melting size  $r_m$  to act as initial nuclei for column growth. When the desorption rate of atoms from the surface increases the growth of clusters is slowed down. Consequently, the probability of cluster growth can only be enhanced by slowing down the embedding of clusters into the matrix via increasing the mobility of clusters which occurs when  $\kappa$  is increased (recall that  $\kappa$  is increased via reduction of the polymer deposition rate  $R_p$ ).

A further effect of increasing the atomic desorption is a reduction of the total number of columns. This is a direct consequence of the enhanced probability of atom re-emission. This effect can also be seen in Fig. 8 which shows a top view of the composite after termination of deposition: clearly the columns grow thicker with higher desorption rates. The second stage is characterized by a relatively small rise of the number of columns with increasing  $\kappa$ . During this stage the columns are steadily growing thicker whereas their aspect ratio remains within a relatively narrow range see Fig. 7(b). This, obviously, implies that the mean column length is also increasing at a comparable rate. Also, the diameter of the columns increases when the desorption rate is increased.

The third stage can be identified by an abrupt increase of the total number of columns. From Fig. 7(c) one can see

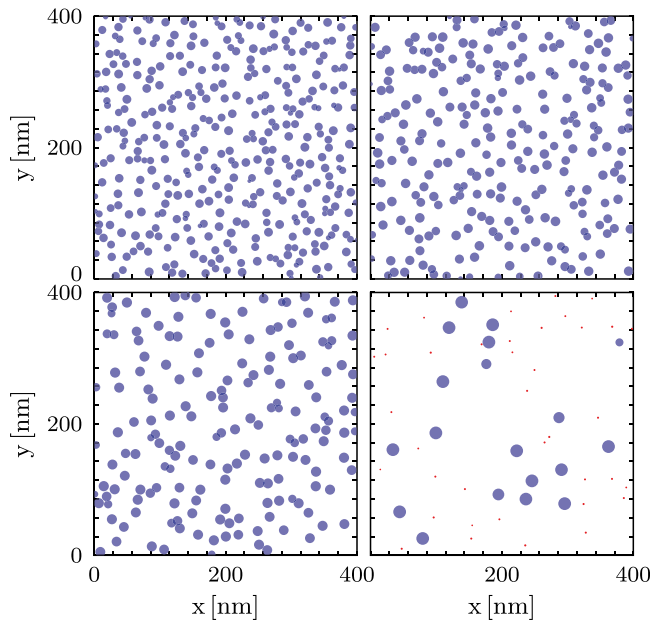


FIG. 8. Top view of the surface microstructure after termination of both deposition processes for  $\kappa = 0.4$  and four different evaporation rates. Top left:  $\nu_e = 2.05 \times 10^3 \text{ s}^{-1}$ , top right:  $\nu_e = 4.1 \times 10^3 \text{ s}^{-1}$ , bottom left:  $\nu_e = 8.2 \times 10^3 \text{ s}^{-1}$ , bottom right:  $\nu_e = 1.64 \times 10^4 \text{ s}^{-1}$ . Other parameters are the same as in Fig. 7. Columns (clusters) are depicted as blue (small red) circles.

that the accelerated growth of columns is accompanied by a steep rise of the filling factor, which is more pronounced for higher desorption rates. Our simulations show that this stage comes along with a growing number of columns extending over the whole height of the final composite, resulting in a higher metal coverage of the surface. The mean column diameter is decreasing during this stage due to the increased number of nuclei available for column growth. This gives rise to a significantly higher aspect ratio. Our simulations show that the average height of the nanocolumns is even some nanometers larger than the thickness of the substrate, see Fig. 10, i.e., the majority of the columns extends above the surface. Consequently the incoming atoms are distributed among a larger number of columns compared to the previous stage.

During the fourth growth stage that starts between  $\kappa \approx 3.0$  (blue curve in Fig. 7(c)) and  $\kappa \approx 4.2$  (brown curve), the number and average length of columns remain constant. Only the filling factor and the column diameter increase (and, therefore, the aspect ratio decreases), due to the higher amount of metal atoms impinging on the surface.

## B. Influence of surface diffusion

Fig. 9 shows the same quantities as Fig. 7 for a fixed desorption rate  $\nu_e = 4.92 \times 10^3 \text{ s}^{-1}$ , but different surface diffusion coefficients  $D_1$ . The main effect of increasing  $D_1$  is a shift of the transition from spherical growth to columnar growth to smaller values of  $\kappa$ , see Figs. 9(a) and 9(c). The reason is obviously the accelerated cluster growth caused by a higher mobility. While for slow surface diffusion the cluster growth is dominated by direct impingement of atoms on pre-existing clusters, for fast surface diffusion the probability of two clusters to encounter each other

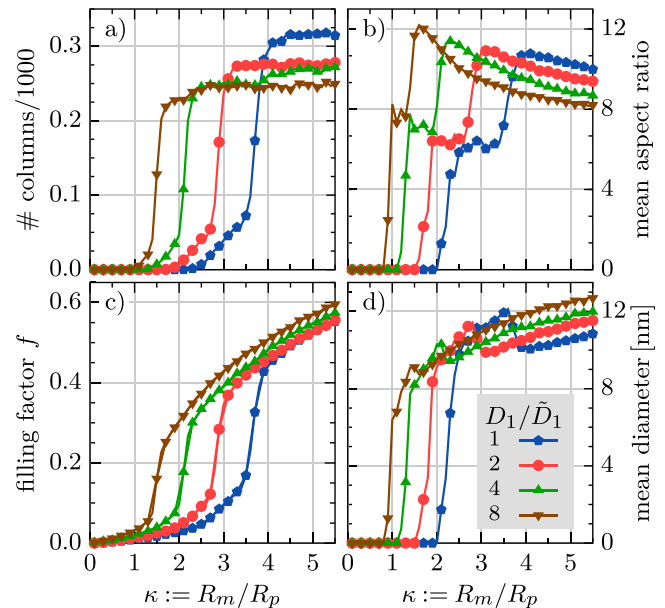


FIG. 9. Same as Fig. 7, but for the case of different surface diffusion coefficients  $D_1$  of monomers. The constant  $\bar{D}_1$  is set to  $1.845 \times 10^{-11} \text{ cm}^2/\text{s}$ . The evaporation rate equals  $\nu_e = 4.92 \times 10^3 \text{ s}^{-1}$ .

during surface diffusion is considerably enhanced. As a consequence, clusters reach the critical nucleus size to induce the columnar growth already for smaller values of  $\kappa$ . Interestingly, the filling factors for higher values of  $\kappa$  ( $\geq 4.4$ ) lie very close together. Our simulations do not show a tendency of the surface diffusion coefficient to influence the filling factor. Other quantities are also weakly affected by the diffusion constant, when columnar growth is observed. Fig. 9(a) shows that for all simulations the number of columns lies between 200 and 300 what corresponds to a column surface density between  $1.63 \times 10^{-3} \text{ nm}^{-2}$  and  $2.12 \times 10^{-3} \text{ nm}^{-2}$ , where the density is higher the lower is  $D_1$ . As one can see in Fig. 9(d), the thickness of the

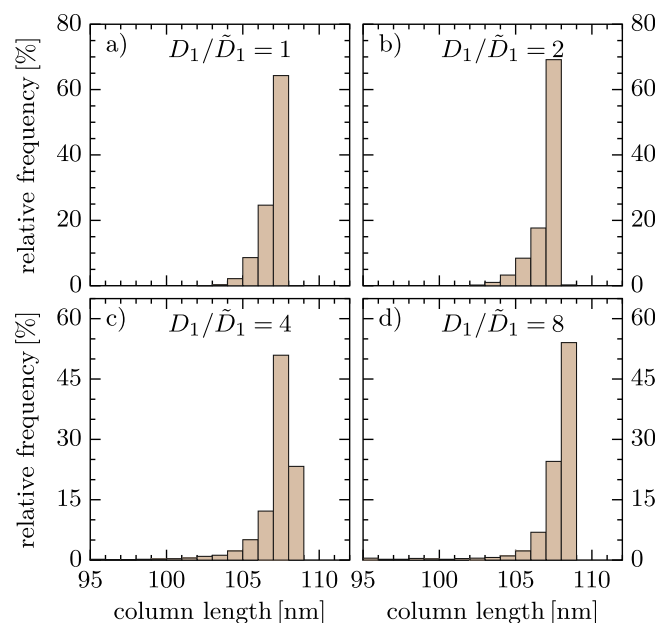


FIG. 10. Distribution of column lengths for  $\kappa = 4.0$  depicted in a histogram with a resolution of 1 nm. The parameter set is the same as in Fig. 9.

columns follows the opposite trend: A higher surface diffusivity leads to thicker columns, which is not surprising since clusters grow faster. The aspect ratio shows the opposite trend, cf. Fig. 9(b). This implies that, in the simulated range of  $D_1$ , the average length of the nanocolumns stays nearly constant.

Fig. 10 shows the distribution of column lengths after termination of both deposition processes, for four different surface diffusion coefficients. All columns extend some nanometers above the surface (which is located at 100 nm). Furthermore, for all values of  $D_1$  the length distribution is very narrow with a maximum at about 108 nm.

## V. CONCLUSION

In this paper, we presented new experimental data on the formation of magnetic Fe-Co-Ni nanocolumns in a Teflon AF matrix during co-evaporation of the metallic and organic components. We extended the deposition to low temperatures and reported also magnetic properties. In particular, we reported that the nanocolumns contain domain walls perpendicular to the column axis which is also the easy axis of magnetization.

The formation of the nanocolumns was, furthermore, modeled in terms of kinetic Monte Carlo simulations which show excellent agreement with the key experimental observations, such as the column diameter, the aspect ratio and the filling factor. A particular highlight of the simulations is that they provide a thorough physical understanding of the correlation between the transition from spherical cluster growth to nanocolumn formation, including the steep increase of the metallic filling factor, in terms of the interplay of a few elementary processes. To the best of our knowledge, such simulations have not been published before. It was shown that, in addition to a low metal condensation coefficient on the organic surface and a high deposition rate ratio of metallic versus organic components, the solidification of the spherical nanoparticles at a critical radius has to be taken into account.

With respect to applications, the results indicate how to tailor the nanocolumnar structure in the matrix and which parameter ranges are accessible. The implications are not restricted to organic matrices but should hold for designing functional metal-dielectric nanocomposites in general, particularly with respect to magnetic and plasmonic applications. The magnetization of the nanocolumns can be tuned, for instance, via their length and separation. Moreover, a magnetic field can be applied during deposition to orient the easy axis of magnetization. In particular, composites containing oriented magnetic nanoparticles with a small aspect ratio are very interesting for high-frequency magnetic materials up to the GHz range.<sup>32</sup>

## ACKNOWLEDGMENTS

This work was supported by the German Research Foundation (DFG) within the framework of the Collaborative

Research Center SFB Transregio 24, Project Nos. A5, A7, and B13. The authors would like to thank Stefan Rehders for setting up the evaporation chamber and his continuous technical support. The magnetization measurements were performed by Michael Frommberger in the group of Eckhard Quandt.

- <sup>1</sup>H. Greve, A. Biswas, U. Schürmann, V. Zaporozhchenko, and F. Faupel, *Appl. Phys. Lett.* **88**, 123103 (2006).
- <sup>2</sup>W. Caseri, *Macromol. Rapid Commun.* **21**, 705 (2000).
- <sup>3</sup>M. Elbahri, M. Hedayati, V. Kiran Chakravadhanula, M. Jamali, T. Strunskus, V. Zaporozhchenko, and F. Faupel, *Adv. Mater.* **23**, 1993 (2011).
- <sup>4</sup>H. Greve, C. Pochstein, H. Takele, V. Zaporozhchenko, F. Faupel, A. Gerber, M. Frommberger, and E. Quandt, *Appl. Phys. Lett.* **89**, 242501 (2006).
- <sup>5</sup>V. Zaporozhchenko, R. Podschun, U. Schürmann, A. Kulkarni, and F. Faupel, *Nanotechnology* **17**, 4904 (2006).
- <sup>6</sup>A. Hahn, T. Stöver, G. Paasche, M. Löbner, K. Sternberg, H. Rohm, and S. Barcikowski, *Adv. Eng. Mater.* **12**, B156 (2010).
- <sup>7</sup>F. Faupel, V. Zaporozhchenko, T. Strunskus, and M. Elbahri, *Adv. Eng. Mater.* **12**, 1177 (2010).
- <sup>8</sup>G. Carotenuto, L. Nicolais, B. Martorana, and P. Perlo, in *Metal-Polymer Nanocomposites*, edited by L. Nicolais and G. Carotenuto (John Wiley & Sons, Inc., 2005), p. 155.
- <sup>9</sup>T. Hanemann and D. Szabó, *Materials* **3**, 3468 (2010).
- <sup>10</sup>A. Heilmann, J. Werner, M. Kelly, B. Holloway, and E. Kay, *Appl. Surf. Sci.* **115**, 365 (1997).
- <sup>11</sup>H. Biederman, *Vacuum* **59**, 594 (2000).
- <sup>12</sup>U. Schürmann, W. Hartung, H. Takele, V. Zaporozhchenko, and F. Faupel, *Nanotechnology* **16**, 1078 (2005).
- <sup>13</sup>H. T. Beyene, V. Chakravadhanula, C. Hanisch, T. Strunskus, V. Zaporozhchenko, M. Elbahri, and F. Faupel, *Plasmonics* **7**, 107 (2012).
- <sup>14</sup>F. Faupel, A. Thran, V. Zaporozhchenko, M. Kiene, T. Strunskus, and K. Behnke, "Stress-induced phenomena in metallization," *AIP Conf. Proc.* **491**, 201 (1999).
- <sup>15</sup>V. Zaporozhchenko, T. Strunskus, K. Behnke, and F. Faupel, in *Proc. Euromat 99, 9, Interface Controlled Materials: Fifth International Workshop*, edited by M. Rühle and H. Gleiter (Wiley-VCH, Weinheim, 2000), p. 24.
- <sup>16</sup>V. Zaporozhchenko, T. Strunskus, K. Behnke, C. von Bechtolsheim, M. Kiene, and F. Faupel, *J. Adhes. Sci. Technol.* **14**, 467 (2000).
- <sup>17</sup>A. Thran, M. Kiene, V. Zaporozhchenko, and F. Faupel, *Phys. Rev. Lett.* **82**, 1903 (1999).
- <sup>18</sup>H. Takele, H. Greve, C. Pochstein, V. Zaporozhchenko, and F. Faupel, *Nanotechnology* **17**, 3499 (2006).
- <sup>19</sup>A. Biswas, P. Karulkar, H. Eilers, M. G. Norton, D. Skorski, C. Davitt, H. Greve, U. Schürmann, V. Zaporozhchenko, and F. Faupel, *Vac. Technol. Coat.* **7**, 54 (2006).
- <sup>20</sup>B. Silverman, *Macromolecules* **24**, 2467 (1991).
- <sup>21</sup>A. Thran and F. Faupel, *Defect Diffus. Forum* **143–147**, 903 (1997).
- <sup>22</sup>F. Faupel, R. Willecke, and A. Thran, *Mater. Sci. Eng. R.* **22**, 1 (1998).
- <sup>23</sup>L. Rosenthal, A. Filinov, M. Bonitz, V. Zaporozhchenko, and F. Faupel, *Contrib. Plasma Phys.* **51**, 971 (2011).
- <sup>24</sup>M. Bonitz, L. Rosenthal, K. Fujioka, V. Zaporozhchenko, F. Faupel, and H. Kersten, *Contrib. Plasma Phys.* **52**, 890 (2012).
- <sup>25</sup>A. Biswas, Z. Marton, J. Kanzow, J. Kruse, V. Zaporozhchenko, F. Faupel, and T. Strunskus, *Nano Lett.* **3**, 69 (2003).
- <sup>26</sup>H. Greve, Ph.D. dissertation, Christian-Albrechts-Universität, Kiel, Germany, 2007.
- <sup>27</sup>V. Zaporozhchenko, K. Behnke, T. Strunskus, and F. Faupel, *Surf. Sci.* **454–456**, 412 (2000).
- <sup>28</sup>H. Takele, S. Jebiril, T. Strunskus, V. Zaporozhchenko, R. Adelung, and F. Faupel, *Appl. Phys. A* **92**, 345 (2008).
- <sup>29</sup>B. D. Cullity and C. D. Graham, *Introduction to Magnetic Materials, Second Edition* (Wiley, Hoboken, 2008).
- <sup>30</sup>G. J. Strijkers, J. H. J. Dalderop, M. A. A. Broeksteeg, H. J. M. Swagten, and W. J. M. de Jonge, *J. Appl. Phys.* **86**, 5141 (1999).
- <sup>31</sup>P. Jensen, *Rev. Mod. Phys.* **71**, 1695 (1999).
- <sup>32</sup>R. Ramprasad, P. Zurcher, M. Petras, M. Miller, and P. Renaud, *J. Appl. Phys.* **96**, 519 (2004).